*Acta Biochim Biophys Sin* 2022, 54(9): 1365–1375
https://doi.org/10.3724/abbs.2022128
Advance Access Publication Date: 20 September 2022
Original Article

Original Article

# lncRNA TUG1 regulates hyperuricemia-induced renal fibrosis in a rat model

**Ying Zhang[1,†], Haizhen Zhang[1,†], Langtao Hu[1,†], Jiali Wei[1,*], and Chunyang Ma[2,*]**

[1]Department of Nephrology, Hainan General Hospital (Hainan Affiliated Hospital of Hainan Medical University), Haikou 570311, China, and [2]Department of Neurosurgery, First Affiliated Hospital of Hainan Medical University, Haikou 570100, China

[†]These authors contributed equally to this work.

*Correspondence address. Tel: +86-18689957525; E-mail: Weijiali56420@163.com (J.W.) / Tel: +86-13876789480; E-mail: MAMachunyangoij@outlook.com (C.M.)

Received 2 November 2021 Accepted 2 March 2022

**Abstract**

Renal fibrosis is most common among chronic kidney diseases. Molecular studies have shown that long noncoding RNAs (lncRNAs) and microRNAs (miRNAs) participate in renal fibrosis, while the roles of lncRNA taurine upregulated gene 1 (TUG1) and miR-140-3p in hyperuricemia-induced renal fibrosis remain less investigated. In this study, a rat hyperuricemia model is constructed by oral administration of adenine. TUG1, miR-140-3p, and cathepsin D (CtsD) expression levels in rat models are measured. After altering TUG1, miR-140-3p, or CtsD expression in modelled rats, biochemical indices, including uric acid (UA), serum creatine (SCr), blood urea nitrogen (BUN), and 24-h urine protein are detected, pathological changes in the renal tissues, and renal fibrosis are examined. In renal tissues from hyperuricemic rats, TUG1 and CtsD are upregulated, while miR-140-3p is downregulated. Inhibiting TUG1 or CtsD or upregulating miR-140-3p relieves renal fibrosis in hyperuricemic rats. Downregulated miR-140-3p reverses the therapeutic effect of TUG1 reduction, while overexpression of CtsD abolishes the role of miR-140-3p upregulation in renal fibrosis. Collectively, this study highlights that TUG1 inhibition upregulates miR-140-3p to ameliorate renal fibrosis in hyperuricemic rats by inhibiting CtsD.

**Key words** hyperuricemia, renal fibrosis, taurine upregulated gene 1, miR-140-3p, cathepsin D

## Introduction

Chronic kidney disease (CKD) is a common health issue that induces gradual and irreversible renal tissue injury, nephron loss and dysfunction and is the 3rd highest cause of premature mortality (82%), second only to AIDS and diabetes mellitus [1]. Hyperuricemia is a CKD characterized by an excessively increased urate concentration resulted from overproduction, gut underexcretion, or renal underexcretion [2]. Renal interstitial fibrosis (RIF) is the final common outcome of CKD and is characterized by an inflammatory reaction, extracellular matrix deposition, epithelial-mesenchymal transition (EMT), microvascular rarefaction, and fibroblast activation and proliferation [3]. The central cellular event in RIF is myofibroblast accumulation, which is mainly responsible for the deposition of an extracellular matrix under pathological conditions [4]. There is still no effective therapeutic strategy to prevent and cease the development of RIF [5]. Thus, it is of significance to investigate the molecular mechanisms implicated in renal fibrosis and to explore effective treatments.

Long noncoding RNAs (lncRNAs) are eukaryotic cell genome-encoded transcripts lacking an apparent open reading frame and do not encode proteins [6]. It has been reported that lncRNA MANTIS attenuates uremic toxin-induced injury in CKD and end-stage renal disease [7], while LINC00963 activates RIF and oxidative stress injury in chronic renal failure [8]. Taurine upregulated gene 1 (TUG1) is a newly found lncRNA implicated in acute kidney injury [9], and it has been believed to be involved in diabetic nephropathy [10,11]. Moreover, *TUG1* silencing has been reported to reduce the EMT of renal tubular epithelial cells, offering a promising target for RIF [12]. MicroRNAs (miRNAs) are small noncoding RNAs that can negatively modulate gene expression [13]. miR-140 plays an important role in renal fibrosis[14], and miR-140-3p can regulate fibrogenesis of hepatic stellate cells [15]. Cathepsin D (CtsD) is a lysosomal aspartic protease in the pepsin superfamily [16]. It has been revealed that CtsD regulates renal fibrosis in murine CKD [17] and is involved in acute kidney injury [18]. However,

the functional roles of the TUG1/miR-140-3p/CtsD axis in hyperuricemia-induced renal fibrosis have not yet been fully confirmed.

In this study, we identified the role of the TUG1/miR-140-3p/CtsD axis in hyperuricemia-induced renal fibrosis in a rat model, and inferred that there is a binding region between TUG1 and miR-140-3p, along with miR-140-3p and CtsD according to the bioinformatics analysis. TUG1 may sponge miR-140-3p to affect CtsD expression and mediate renal fibrosis development.

## Materials and Methods

### Ethics statement

All animal experiments were performed following the Guide to the Management and Use of Laboratory Animals issued by the National Institutes of Health (NIH, Bethesda, USA). The protocols were approved by the Institutional Animal Care and Use Committee of Hainan Affiliated Hospital of Hainan Medical University.

### Experimental animals and grouping

Specific pathogen-free grade male Sprague Dawley rats (230 ± 20 g, 3 months old) purchased from the Medical Experimental Animal Center of Hainan Province (Hainan, Haikou, China) were adaptively fed for 1 week. The HN rat model was established by oral a gavage of adenine (0.1 g/kg; Biosharp Life Science, Hefei, China) and potassium oxalate (1.5 g/kg; Macklin Biochemical Co., Ltd, Shanghai, China) in 0.5% carboxymethycellulose sodium (CMCe-Na; Chron Chemicals Co., Ltd, Chengdu, China) every day for a total of 3 weeks [19,20]. Rats in the sham group were treated with an equal volume of normal saline every day.

The model rats were injected with 100 μL of TUG1 overexpression vector (Oe-TUG1), NC of TUG1 overexpression vector (Oe-NC), TUG1 low expression vector (sh-TUG1), NC of TUG1 low expression vector (sh-NC), miR-140-3p antagomir, antagomir NC, miR-140-3p agomir, agomir NC, CtsD overexpression vector (oe-CtsD), NC of CtsD overexpression vector (oe-NC), CtsD low expression vector (sh-CtsD) or NC of CtsD low expression vector (sh-NC) through the caudal vein every week for 3 weeks. In this study, lentivirus vector containing TUG1, CtsD, TUG1 shRNA, CtsD shRNA, miR-140-3p agomir or miR-140-3p antagomir, and the corresponding NCs were all designed and constructed by GenePharma (Shanghai, China), and the titer of the recombinant lentivirus was $1 \times 10^8$ plaque-forming units (pfu)/mL. Detailed sequence information was showed as follows: sh-TUG1 (5′-GTCTGCATTGAGGATATAG-3′), sh-NC (5′-CCTCTAGGTAAGCATAATTTT-3′), miR-140-3p antagomir (5′-CCGUGGUUCUACCCUGUGGUA-3′), antagomir NC (5′-CAGUACUUUUGUGUAGUACAAA-3′), miR-140-3p agomir (5′-UACCACAGGGUAGAACCACGG-3′), agomir NC (5′-UUUGUACUACACAAAAGUACUG-3′), sh-CtsD (5′-CCGGCCTCTTATCCAGGGTGAGTATCTCGAGATACTCACCCTGGATAAGAGGTTTTT-3′) and sh-NC (5′-CCGGCCTTTGATGCACGGGAACAATCTCGAGATTGTTCCCGTGCATCAAAGGTTTTTG-3′). Sequence information of pcDNA3.1-TUG1/Oe-TUG1, pcDNA3.1/Oe-NC, pcDNA3.1-CtsD/oe-CtsD, and pcDNA3.1 empty vector/oe-NC are provided in Supplementary Material S1.

### Urine test

At the 6th week of the experiment, rats were weighed and put into metabolic cages and only supplied with water. Urine was collected over 24 h, and the volume was recorded. The urine was centrifuged at 1358 *g* for 15 min, and the supernatant was stored at –20°C. The 24-h urinary protein was determined by the Coomassie brilliant blue method.

### Serological determination

At the 6th week of the experiment, blood was collected from the rat tail vein after the urine test and centrifuged at 1358 *g* for 15 min, and the supernatant was preserved at –20°C. Serum creatine (SCr), blood urea nitrogen (BUN), and uric acid (UA) were measured with an AU2700 fully automatic biochemical analyser (Olympus, Tokyo, Japan).

### Sample preparation

At the 6th week of the experiment, rats were anesthetized by intraperitoneal injection of 1% pentobarbital sodium (Sigma, St Louis, USA), and both kidneys were isolated. After the renal capsule was removed, the right kidney was fixed in 15% neutral formalin (Sigma), paraffin-embedded, and cut into 4-μm sections for hematoxylin-eosin (HE) staining and Masson staining, as well as alpha-smooth muscle actin (α-SMA) and type I collagen (COL-I) immunohistochemical staining. The left kidney was used for reverse transcription quantitative polymerase chain reaction (qRT-PCR) and western blot analysis.

### HE staining

Paraffin sections of renal tissue were subject to HE staining as previously described [21]. Sections were sealed with neutral gum and observed under a light microscope (Olympus, Tokyo, Japan).

### Masson staining

Sections were successively soaked in xylene and ethanol and then incubated with saturated picric acid mordant overnight. After treatment with potassium dichromate at 50°C for 45 min, the sections were stained with hematoxylin, differentiated with hydrochloric alcohol, counterstained with Masson dye for 45 min, rinsed with 1% glacial acetic acid aqueous solution, and sealed with neutral balsam. Five optical fields from each section were selected and examined with a light microscope (Olympus, Tokyo, Japan) at magnification of 200 ×, and the green fibrous area indicates positive staining. RIF index (%) = (fibrosis area/total area of kidney) × 100% [22].

### Immunohistochemical staining

The sections were heated at 60°C for 30–60 min, successively immersed in xylene and ethanol, and then boiled in 0.01 M sodium citrate buffer (pH 6.0) for 3 min, incubated with 3% $H_2O_2$ for 15 min, followed by incubation with primary antibodies against α-SMA or COL-I (1:200; Sigma) at 4°C overnight. Subsequently, sections were incubated with goat anti-rabbit immunoglobulin G (IgG) antibody-horseradish peroxidase polymer for 40 min, developed using diaminobenzidine, stained with hematoxylin for 5 min, and differentiated with 1% hydrochloric alcohol for 10 s. After dehydration and clearance, the sections were sealed with neutral balsam, and images were captured with a microscope (Olympus, Tokyo, Japan) and analysed using the Image-ProPlus6.0 software (MediaCybernetics, Silver Spring, USA).

### qRT-PCR

Total RNA in rat renal tissues was extracted using TRIzol (TaKaRa,

Dalian, China), and reverse transcription was performed using PrimeScriptTM RT reagent Kit (TaKaRa) or miRcute Plus miRNA First-Strand cDNA Kit (Tiangen, Beijing, China). qRT-PCR was conducted using SYBR Premix ExTaq kit (TaKaRa) or miRcute Plus miRNA qPCR (SYBR Green) Kit (Tiangen). For miRNA, PCR programs were set up as follows: initial denaturation for 5 min at 95°C, followed by 40 cycles with denaturation for 20 s at 95°C and annealing for 34 s at 60°C. For lncRNA and mRNA, PCR programs were set up as follows: 5 min at 95°C, followed by 40 cycles with 5 s at 95°C and 31 s at 60°C. The data were analysed by the $2^{-\Delta\Delta Ct}$ method [23] with *U6* as the internal control of miRNA and glyceraldehyde phosphate dehydrogenase (*GAPDH*) as the internal control of lncRNA and mRNA. The primer sequences are shown in Table 1.

### Western blot analysis

Renal tissues were homogenized in radioimmunoprecipitation assay buffer (MerckMillipore, Burlington, USA) supplemented with protease and phosphatase inhibitors (MerckMillipore) on ice, and protein concentration assays and western blot analyses were conducted based on previous descriptions [24]. The protein concentrations were measured using BCA Assay kit (Pierce, Rockford, USA). For western blot analysis, protein extracts were separated by 10% SDS-PAGE and transferred to the nitrocellulose membranes. The membranes were incubated with primary antibodies against zonula occludens-1 (ZO-1, 1:500, ab96587; Abcam, Cambridge, USA), occludin (1:1000, ab31721; Abcam), CtsD (1:1000, ab826; Abcam), and GAPDH (1:2500, ab9485; Abcam) at 4°C overnight, and then with horseradish peroxidase-conjugated secondary antibody (1:2000; sc-2004, Santa Cruz Biotechnology, Dallas, USA) for 1 h. The protein bands were visualized and quantified using ImageJ software (NIH, Bethesda, USA).

**Table 1. Sequence of primers used in this study**

| Gene | Primer sequence |
|---|---|
| *TUG1* | F: 5′-TTAAGGGCCAAACGCCATCA-3′ |
| | R: 5′-GGGCCAGTTGGGTATAGCAG-3′ |
| *miR-140-3p* | F: 5′-TACCACAGGGTAGAACCACGG-3′ |
| | R: 5′-CCACAGGGTAGAACCACGG-3′ |
| *U6* | F: 5′-ATTGGAACGATACAGAGAAGATT-3′ |
| | R: 5′-GGAACGCTTCACGAATTTG-3′ |
| *CtsD* | F: 5′-TACTCAAGGTATCGCAGGGTG-3′ |
| | R: 5′-CCAATGAAGACATCGCCCAG-3′ |
| *GAPDH* | F: 5′-ATGCTGCCCTTACCCCGG-3′ |
| | R: 5′-TTACTCCTTGGAGGCCATGTAGG-3′ |
| *TGF-β1* | F:5′-CTTCAGCTCCACAGAGAAGAACTGC-3′ |
| | R:5′-CACGATCATGTTGGACAACTGCTCC-3′ |
| *TIMP-1* | F:5′-TCCTCTTGTTGCTATCACTGATAGCTT-3′ |
| | R:5′-CGCTGGTATAAGGTGGTCTCGTT-3′ |
| *NGAL* | F:5′-CAGGACTCCACCTCAGACCT-3′ |
| | R:5′-CCAGGCCTACCACATACCAC-3′ |
| *KIM-1* | F:5′-AGAGAGAGCAGGACACAGGCTT-3′ |
| | R:5′-ACCCGTGGTAGTCCCAAACA-3′ |

F, forward; R, reverse; TUG1, Taurine up-regulated gene 1; CtsD, Cathepsin D; GAPDH, glyceraldehyde phosphate dehydrogenase; TGF-β1, transforming growth factor-β1; TIMP-1, tissue inhibitor of metalloproteinase 1; NGAL, neutrophil gelatinase-associated lipocalin; KIM-1, kidney injury molecule 1.

### Luciferase reporter assay

Binding sites of TUG1 and CtsD 3′-UTR in miR-140-3p were predicted at https://cm.jefferson.edu/rna22/Precomputed/, and mutated to generate TUG1-MUT (5′-UUUAAGAUCUCAACG-3′) and CtsD-MUT (5′-GUUCUGUUACACAAGU-3′). HEK293T cells (CL-0005; Procell, Wuhan, China) were transfected with 50 ng of recombinant reporter plasmids (TUG1-WT, TUG1-MUT, CtsD-WT or CtsD-MUT), 50 ng of a Renilla normalization control (Promega, Madison, USA), and 100 nM of miR-140-3p mimic (GenePharma, the sequence of the miR-140-3p mimic was 5′-UACCACAGGGUA GAACCACGG-3′) using LT1 Transfection Reagent (Mirus, Madison, USA) following the manufacturer's instructions. At 48 h after the transfection, luciferase detection was conducted using a luciferase reporter assay kit (Promega).

### Pull-down assay with a biotinylated DNA probe

The biotinylated DNA probe complementary to miR-140-3p was synthesized by GenePharma and dissolved in 500 μL of lysis buffer (0.5 M NaCl, 20 mM Tris-HCl, pH 7.5, and 1 mM ethylene diamine tetraacetic acid). The probe was incubated with magnetic beads coated with streptavidin (Thermo Fisher Scientific, Waltham, USA) at 25°C for 3 h, and the cell lysate was incubated with probe-coated beads. RNA was eluted and extracted for PCR.

### Isolation of RNA-induced silencing complex (RISC)-associated RNA

HEK293T cells were transfected with miR-140-3p agomir or agomir-NC using Lipofectamine3000 Transfection Reagent (Thermo Fisher Scientific) and grew to 80% confluency. Then, 1% formalin-fixed cells were lysed using NETN buffer (50 mM Tris, pH 8.0, 1 mM EDTA, 150 mM NaCl, 0.5% NP-40) and cultured with Dyna beads Protein A (Invitrogen, Carlsbad, USA) supplemented with IgG or anti-Pan-Ago, clone 2A8 antibody (Millipore). After proteinase K digestion, the immunoprecipitated RNA was extracted using phenol/chloroform/isopropyl alcohol, purified using ethanol and glycogen, and treated with DNase I (Invitrogen).

### Statistical analysis

All data analyses were conducted using SPSS 21.0 software (IBM. Armonk, USA). Data are presented as the mean ± standard deviation. The *t* test was performed for comparisons between two groups, and one-way analysis of variance (ANOVA) was performed for comparisons among multiple groups. A $P$ value of $< 0.05$ was indicative of statistically significant difference.

## Results

### Hyperuricemia induces renal fibrosis in a rat model

Oral administration of adenine was used to establish a rat renal fibrosis model [19]. Urine test showed that the 24-h urine protein, UA, BUN, and SCr levels were increased, which indicated that the rat model of renal fibrosis was constructed successfully (Figure 1A–D). As observed by HE staining, there were no obvious pathological changes in the renal tissue of rats from the sham group, and the rats had clear glomerular epithelium, without swelling and atrophy, while there were wider interstitial space, inflammatory cell infiltration, expansion of glomerular capillaries, and renal tubular cell atrophy and necrosis in the modelled rats; rats in the model

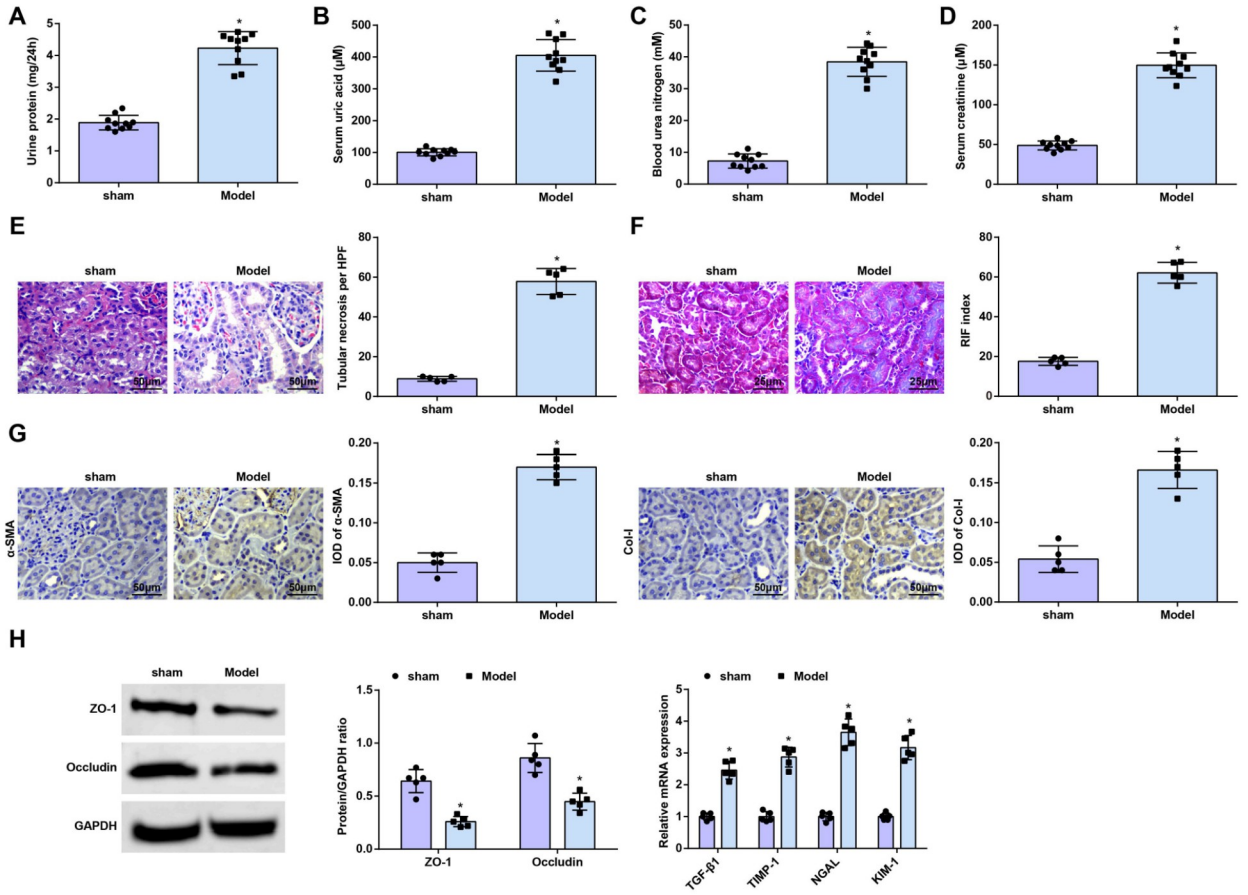


**Figure 1. Hyperuricemia induces renal fibrosis in a rat model** (A) Urine protein of rats. (B) UA of rats. (C) BUN of rats. (D) SCr of rats. (E) Pathological changes and score of rats. (F) Fibrosis degree and renal fibrosis index in rat renal tissues. (G) α-SMA and COL-I content in rat renal tissues. (H) Protein expressions of ZO-1 and occludin, and mRNA expression of TGF-β1, TIMP-1, NGAL, and KIM-1 in rat renal tissues. Data are expressed as the mean ± standard deviation. *$P < 0.05$ vs the sham group.

group had higher pathological scores (Figure 1E).

Rat renal fibrosis was observed by Masson staining: in the sham group, tubules and glomeruli were normal in size and morphology, and pathological changes such as inflammatory cell infiltration and fibrosis were not found. In the model group, there was glomerular compensatory hypertrophy, poor vascular patency in the partial capillary, tubular dilation, partial tubular epithelial cell loss, and epithelial cellular degeneration; in the renal interstitium, diffuse mononuclear cells, lymphocyte infiltration, fibroblast hyperplasia, light green collagenous fibers, and obvious fibrosis were found. RIF was higher in the model rats than in the sham-operated rats (Figure 1F).

The results of immunohistochemical staining suggested that modelled rats showed higher α-SMA and COL-I expression levels, and positive staining was mainly distributed at the renal interstitium, partial fibroblasts, and cytoplasm of tubular epithelial cells (Figure 1G). ZO-1 is a highly expressed tight junction protein that forms a component of the glomerular filtration barrier throughout podocyte differentiation [25]. Podocyte-specific knockout of ZO1 was found to induce foot process disappearance and SD disruption, which resulted in proteinuria and renal failure. EMT plays an important role in kidney development and fibrosis, and occludin can be used as an epithelial cell marker [26,27]. Analysis of ZO-1 and occludin protein expression revealed that ZO-1 and occludin were downregulated in modelled rats (Figure 1H). Meanwhile, RT-qPCR results indicated that transforming growth factor-β1 (TGF-β1), tissue inhibitor of metalloproteinase 1 (TIMP-1), neutrophil gelatinase-associated lipocalin (NGAL), and kidney injury molecule 1 (KIM-1) mRNA expression levels were elevated in modelled rats. All these data indicated that hyperuricemia induced renal fibrosis in rats.

## TUG1 inhibition attenuates renal fibrosis, while TUG1 overexpression aggravates renal fibrosis in hyperuricaemic rats

To explore the effect of TUG1 on renal fibrosis in hyperuricemic rats, qRT–PCR was performed to detect TUG1 expression. The results showed that TUG1 expression was increased in modelled rats (Figure 2A), and the increased expression of TUG1 was suppressed by sh-TUG1 or further promoted by Oe-TUG1 (Figure 2B). The urine test showed that inhibiting TUG1 decreased the 24-h urine protein, UA, BUN, and SCr levels, while overexpressing TUG1 increased the 24-h urine protein, UA, BUN, and SCr levels (Figure 2C–F).

HE staining revealed a wide interstitial space and a slight inflammatory cell infiltration in the sh-TUG1 group, which were decreased compared with the sh-NC group; wider interstitial space, abundant inflammatory cell infiltration, expansion of glomerular capillaries, renal tubular cell atrophy and necrosis were discovered in the Oe-TUG1 group. These results were in line with the pathological scores (Figure 2G). In Masson staining, decreased

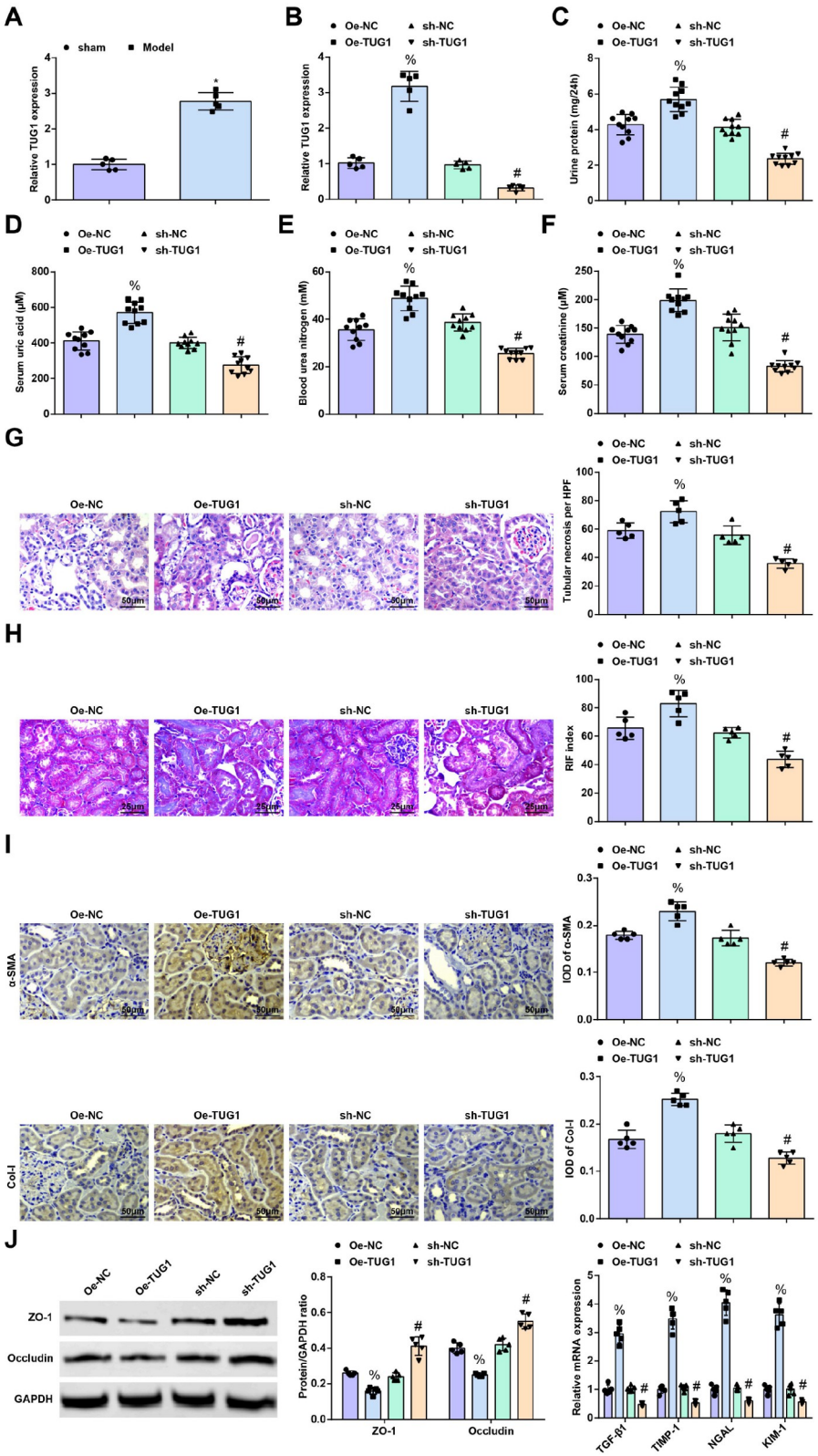


**Figure 2. TUG1 inhibition attenuates renal fibrosis, while TUG1 overexpression aggravates renal fibrosis in hyperuricaemic rats** (A/B) TUG1 expression in rat renal tissues was assessed by qRT-PCR. (C) Urine protein of rats. (D) UA of rats. (E) BUN of rats. (F) SCr of rats. (G) Pathological changes and score of rats. (H, fibrosis degree and renal fibrosis index in rat renal tissues. (I) α-SMA and COL-I contents in rat renal tissues. (J) TGF-β1, TIMP-1, NGAL, KIM-1, ZO-1, and occludin expressions in rat renal tissues. Data are expressed as the mean ± standard deviation. $^{\%}P < 0.05$ vs the sh-NC group; $^{\#}P < 0.05$ vs the Oe-NC group.

tubular dilation, renal interstitial broadening and collagen deposition were observed in the sh-TUG1 group, and the RIF index was reduced; in the Oe-TUG1 group, there was abundant tubular epithelial cell loss and vacuoles, diffuse fibroblast hyperplasia in the renal interstitium, a high degree of fibrosis, significant collagen deposition and an increased RIF index (Figure 2H).

Immunohistochemical staining results showed that α-SMA and COL-I expressions were elevated, transforming growth factor-β1 (TGF-β1), tissue inhibitor of metalloproteinase 1 (TIMP-1), neutrophil gelatinase-associated lipocalin (NGAL), and kidney injury molecule 1 (KIM-1) mRNA expressions were induced, and ZO-1 and occludin protein expression levels were suppressed when TUG1 was upregulated. In contrast, silencing of TUG1 exerted the opposite effects (Figure 2I,J). These data suggested that inhibiting TUG1 improved renal fibrosis in hyperuricaemic rats, while overexpressing TUG1 aggravated renal fibrosis.

## TUG1 targets miR-140-3p

The existence of the target site of TUG1 and miR-140-3p was found in https://starbase.sysu.edu.cn/agoClipRNA.php?source=lncRNA (Figure 3A). Moreover, miR-140-3p was downregulated when TUG1 was overexpressed, while it was upregulated when TUG1 was silenced (Figure 3B). Luciferase reporter assay revealed that cotransfection of WT TUG1 and miR-140-3p mimic reduced the luciferase activity of HEK293T cells, whereas cotransfection of MUT TUG1 and miR-140-3p mimic did not affect the luciferase activity (Figure 3C). RNA pull-down assay confirmed that TUG1 enrichment was enhanced by BiomiR-140-3p-WT but not by BiomiR-140-3p-MUT (Figure 3D), suggesting that TUG1 negatively regulates miR-140-3p.

## Upregulated miR-140-3p ameliorates renal fibrosis, while downregulated miR-140-3p reverses the therapeutic effect of TUG1 knockdown on renal fibrosis

The detection of miR-140-3p expression showed that it was expressed at low levels in the modelled rats. To explore the role of miR-140-3p in renal fibrosis, miR-140-3p agomir was injected into model rats, which successfully elevated miR-140-3p expression in the renal tissues of rats. Meanwhile, to assess whether TUG1 affects renal fibrosis through regulating miR-140-3p, sh-TUG1 + miR-140-3p antagomir were injected in combination into modelled rats, which showed great efficacy to suppress miR-140-3p expression compared to the injection of sh-TUG1 + antagomir NC (Figure 4A,B).

In subsequent experiments, it was found that miR-140-3p upregulation decreased the 24-h urine protein, UA, BUN and SCr contents, pathological scores, RIF index and IOD of α-SMA and COL-I, and TGF-β1, TIMP-1, NGAL, and KIM-1 mRNA expression, but decreased ZO-1 and occludin protein expressions, while downregulation of miR-140-3p reversed the therapeutic effect of TUG1 inhibition on renal fibrosis (Figure 4C–J). These results suggested that upregulated miR-140-3p ameliorates renal fibrosis, while downregulated miR-140-3p reverses the therapeutic effect of TUG1 knockdown on renal fibrosis.

## MiR-140-3p targets CtsD

It was predicted using a bioinformatics website (https://starbase.sysu.edu.cn/agoClipRNA.php?source=mRNA) that binding sites exist between miR-140-3p and CtsD (Figure 5A). Our results showed that CtsD expression in the rat renal tissue was decreased after treatment with miR-140-3p agomir (Figure 5B,C).

It was further confirmed that cotransfection of CtsD-WT and miR-140-3p mimic into HEK293T cells decreased luciferase activity, while cotransfection of CtsD-MUT and miR-140-3p agomir did not change the luciferase activity (Figure 5D). Additionally, CtsD mRNA level in Ago2/RISC was enriched in miR-140-3p mimic-transfected cells (Figure 5E), indicating that miR-140-3p targets CtsD.

## Inhibiting CtsD attenuates renal fibrosis, and CtsD overexpression reverses the therapeutic effect of miR-140-3p elevation on renal fibrosis

To further assess the role of CtsD in renal fibrosis in hyperuricemic

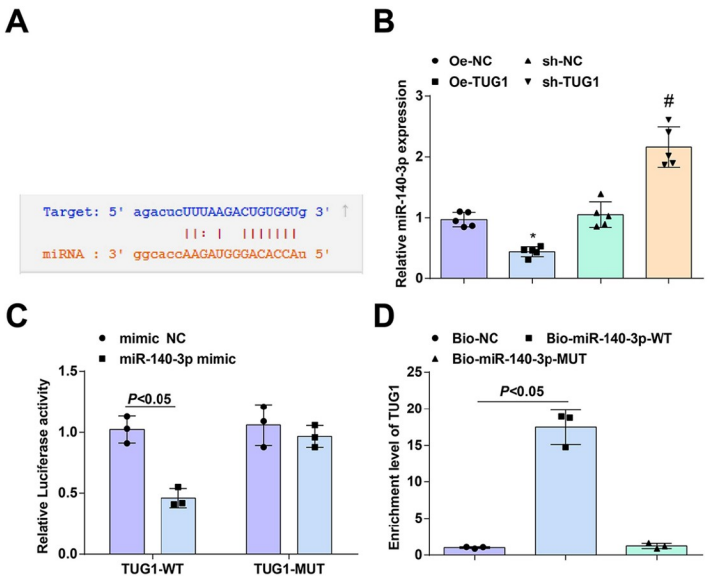


**Figure 3. TUG1 targets miR-140-3p** (A) Binding sites of TUG1 and miR-140-3p were predicted by bioinformatics software. (B) miR-140-3p expression in rat renal tissues. (C) Regulatory relationship between TUG1 and miR-140-3p was confirmed by luciferase activity assay. (D) Target relationship of TUG1 and miR-140-3p was confirmed by RNA pull-down assay. Data are expressed as the mean ± standard deviation. $^{*}P < 0.05$ vs the Oe-NC group; $^{\#}P < 0.05$ vs the sh-NC group.

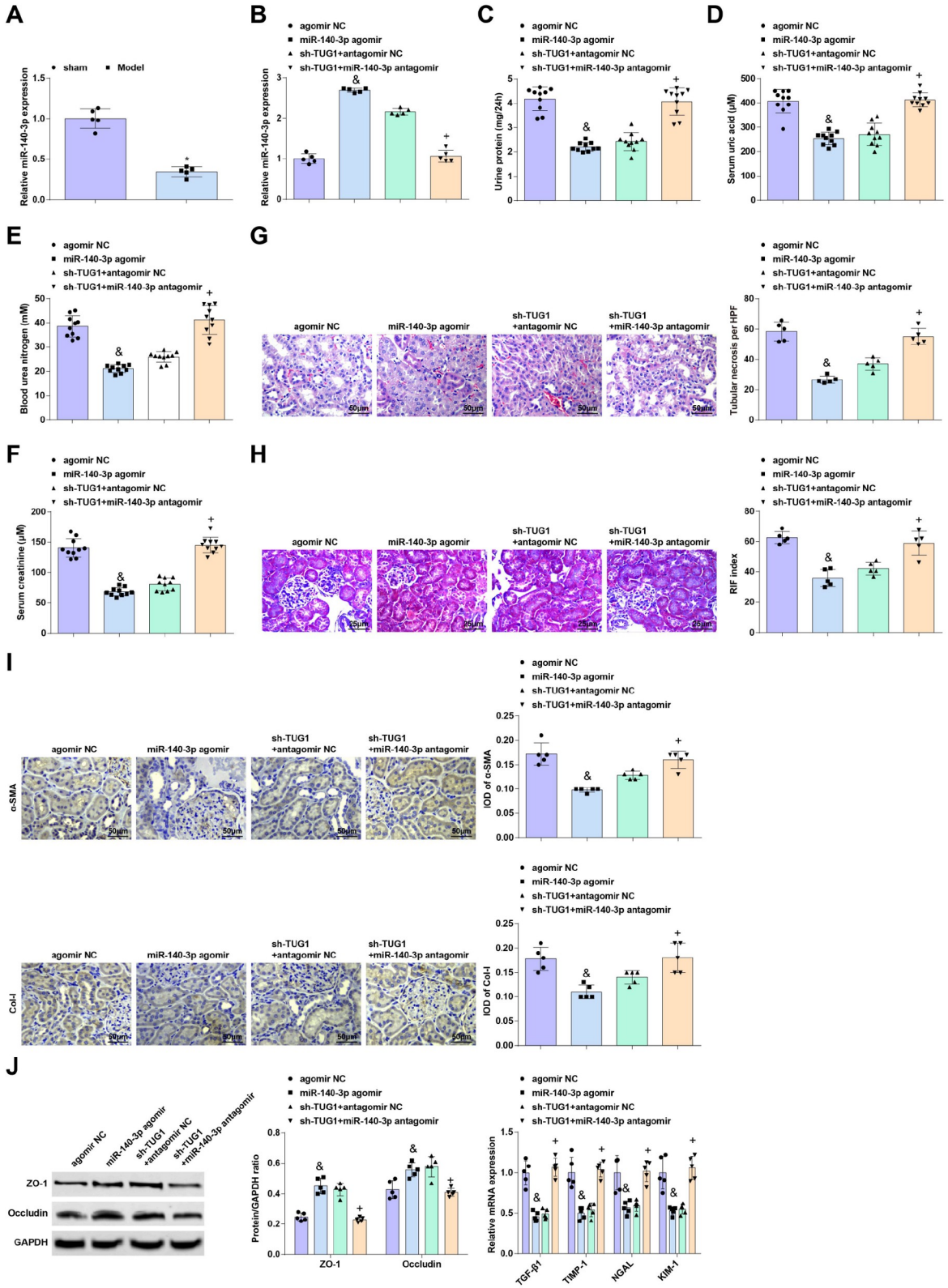


**Figure 4. Upregulated miR-140-3p ameliorates renal fibrosis, while downregulated miR-140-3p reverses the therapeutic effect of TUG1 knockdown on renal fibrosis** (A/B) miR-140-3p expression in rat renal tissues was assessed by qRT-PCR. (C) Urine protein of rats. (D) UA of rats. (E) BUN of rats. (F) SCr of rats. (G) Pathological changes and score of rats. (H) Fibrosis degree and renal fibrosis index in rat renal tissues. (I) α-SMA and COL-I contents in rat renal tissues. (J) TGF-β1, TIMP-1, NGAL, KIM-1, ZO-1, and occludin expression in rat renal tissues. Data are expressed as the mean ± standard deviation. $^{*}P < 0.05$ vs the sham group; $^{\&}P < 0.05$ vs the agomir NC group; $^{+}P < 0.05$ vs the sh-TUG1 + antagomir NC group.

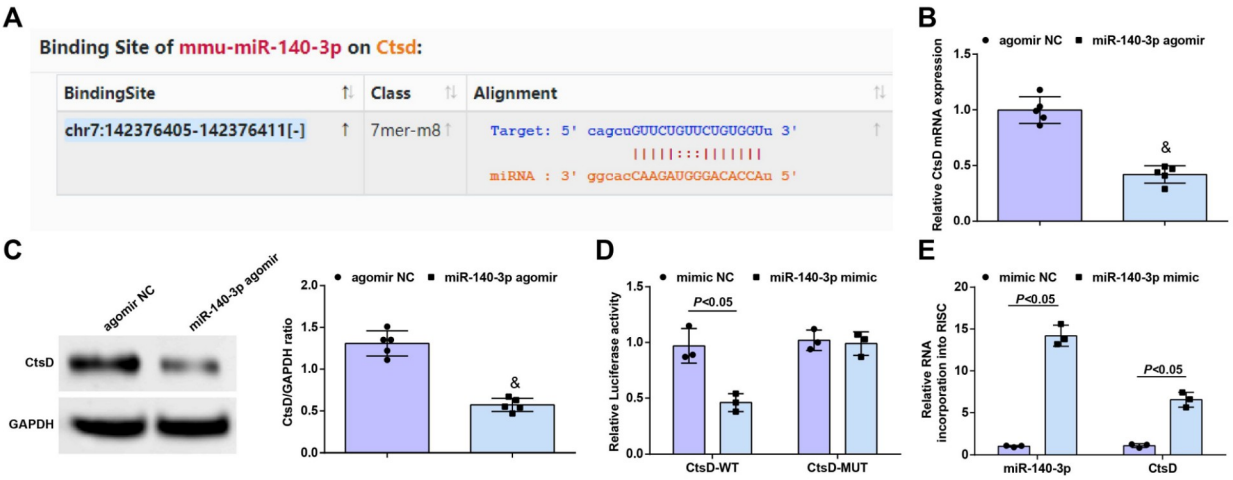


**Figure 5. miR-140-3p targets CtsD** (A) Binding sites of miR-140-3p and CtsD were predicted by bioinformatics software. (B) CtsD mRNA expression in rat renal tissues. (C) Protein expression of CtsD in rat renal tissues. (D) Regulatory relationship between miR-140-3p and CtsD was confirmed by luciferase activity assay. (E) Cells overexpressing miR-140-3p were subject to Ago2/RISC immunoprecipitation with Pan-Ago2 antibody. IgG was used as a negative control, and GAPDH was used as an internal control. Data are expressed as the mean ± standard deviation. $^{\&}P < 0.05$ vs the agomir NC group.

rats, we detected CtsD mRNA and protein expression levels in modelled rats, and found that both levels were high in modelled rats. To determine the involvement of CtsD in renal fibrosis, model rats were treated with sh-CtsD, resulting in a decrease in CtsD expression in the renal tissues (Figure 6A). To confirm that CtsD is involved in the miR-140-3p-mediated progression of renal fibrosis, miR-140-3p agomir and oe-CtsD were injected into model rats, leading to the overexpression of CtsD in renal tissues in comparison to the rats injected with miR-140-3p agomir and oe-NC (Figure 6B).

By a series of assays, we further found that inhibition of CtsD decreased the 24-h urine protein, UA, BUN and SCr levels, the pathological scores, RIF index, levels of α-SMA and COL-I, as well as the TGF-β1, TIMP-1, NGAL, and KIM-1 mRNA expressions, but increased ZO-1 and occludin protein expressions. Meanwhile, CtsD overexpression reversed the therapeutic effect of miR-140-3p elevation on renal fibrosis (Figure 6C–J). These data suggested that CtsD inhibition ameliorates renal fibrosis in hyperuricemic rats, and CtsD overexpression abrogates the therapeutic effect of miR-140-3p upregulation on renal fibrosis.

## Discussion

RIF is a common pathological result of CKD[28]. This study aimed to explore the role of TUG1 in the development of renal fibrosis by regulating miR-140-3p and CtsD, and our results indicated that inhibition of TUG1 was able to improve hyperuricemia-induced renal fibrosis in a rat model by increasing miR-140-3p-targeted suppression of CtsD.

Our study suggested that TUG1 was upregulated in renal tissue from hyperuricemic rats and further revealed that TUG1 knockdown attenuated renal fibrosis, whereas TUG1 induction aggravated renal fibrosis in hyperuricemic rats. Similarly, Xu *et al.* [29] identified that the expression of TUG1 was higher in renal tissue from rats with ischaemia-reperfusion injury and in renal tubular epithelial cells stimulated by oxygen-glucose deprivation. According to a report on liver fibrosis, the upregulation of TUG1 was measured in fibrotic livers of patients, and TUG1 was the inducer of the levels of pro-fibrogenic genes to promote liver fibrosis [30]. In a rat model with myocardial infarction, Sun *et al.* [31] demonstrated that TUG1 expression is increased in myocardial tissue with an increase in cardiac fibrosis, and intervention with TUG1 plays a therapeutic role to reduce cardiac fibrosis. The TUG1 level was confirmed to be elevated during EMT of renal tubular epithelial cells, and the process of EMT could be retarded when TUG1 was inhibited in the setting of RIF [12]. Moreover, lncRNA TUG1 was reported to promote endometrial fibrosis and inflammation in intrauterine adhesions [32].

A novel regulatory mechanism suggested that lncRNAs can act as sponges to adsorb miRNAs, thereby participating in posttranscriptional processing [33], and miR-140-3p is one of the downregulated miRNAs in progressive CKD [34]. In our study, miR-140-3p expression was found to be decreased in the fibrotic renal tissue of hyperuricemic rats, while miR-140-3p induction ameliorated hyperuricemia-induced renal fibrosis, but miR-140-3p reduction suppressed the effects of TUG1 knockdown on hyperuricemia-induced renal fibrosis. Wu *et al.* [15] illustrated that miR-140-3p inhibition suppressed cell proliferation and fibrogenesis in hepatic stellate cells via PTEN-mediated AKT/mTOR signaling. A recent publication also suggested that miR-140-5p could alleviate paraquat-induced pulmonary fibrosis in a mouse model [35].

Finally, our research implied that CtsD is overexpressed in hyperuricemia-induced renal fibrosis, and CtsD silencing is protective for hyperuricemic rats with renal fibrosis. Cocchiaro *et al.* [18] discovered that CtsD expression was upregulated in damaged tubular cells in nephrotoxic and ischemia reperfusion-induced acute kidney injury. Regarding the involvement of CtsD in RIF, it has been demonstrated that CtsD inhibition slows interstitial fibrosis progression following ischemia reperfusion-induced acute kidney injury [18]. It was reported that CtsD inhibition leads to increased collagenolytic activity due to an impairment in lysosomal recycling [17]. Furthermore, CtsD plays multiple roles in apoptosis [18] and inflammation [36]. However, whether CstD participates in fibrosis through these pathways needs to be verified in future investigations.

In summary, our research indicated that TUG1 could sponge miR-

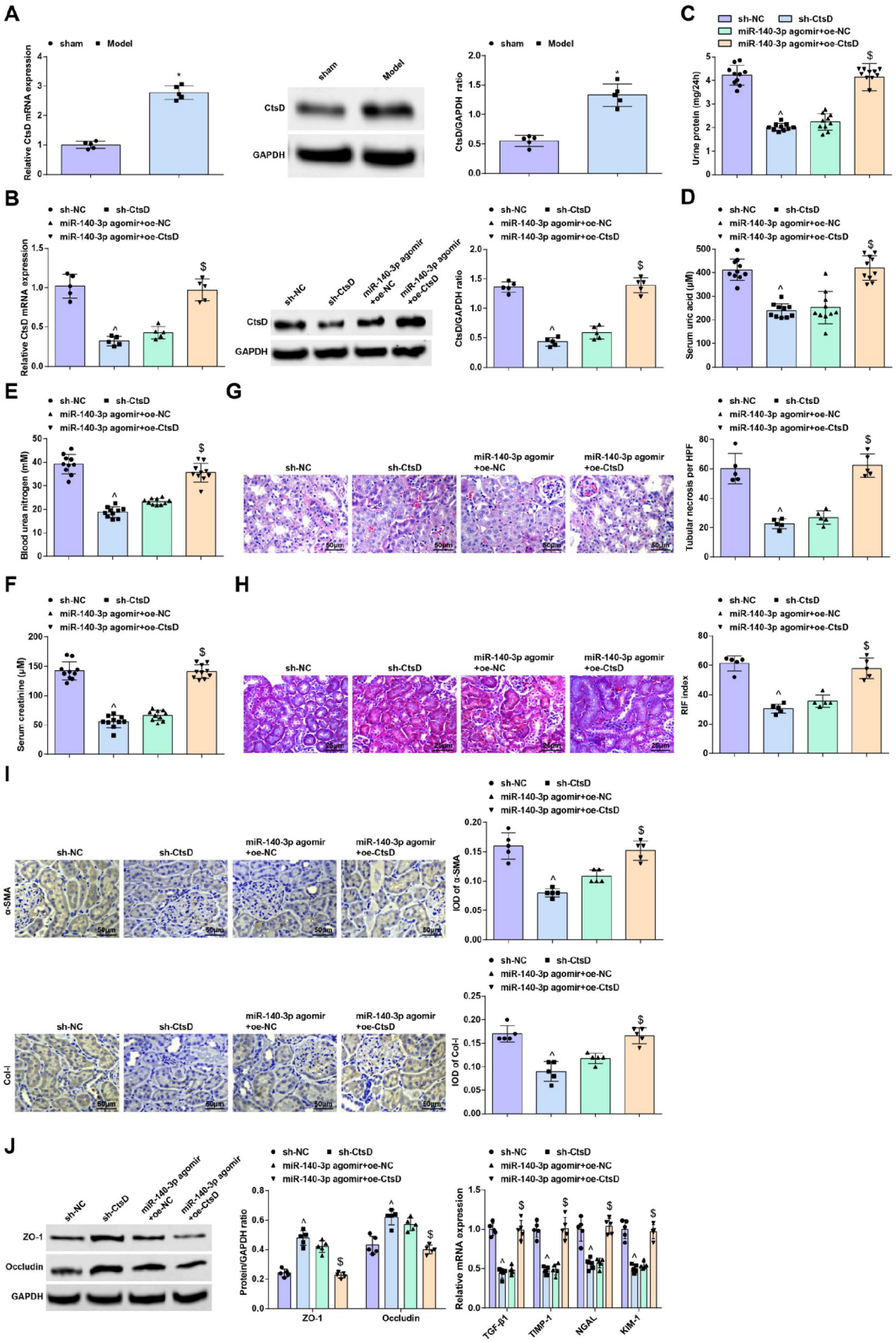


**Figure 6. Inhibiting CtsD attenuates renal fibrosis, and CtsD overexpression reverses the therapeutic effect of miR-140-3p elevation on renal fibrosis** (A,B) CtsD expression in rat renal tissues was assessed by qRT-PCR and western blot analysis. (C) Urine protein of rats. (D) UA of rats. (E) BUN of rats. (F) SCr of rats. (G) Pathological changes and score of rats. (H) Fibrosis degree and renal fibrosis index in rat renal tissues. (I) α-SMA and COL-I contents in rat renal tissues. (J) TGF-β1, TIMP-1, NGAL, KIM-1, ZO-1, and occludin expression in rat renal tissues. Data are expressed as the mean ± standard deviation. $^{*}P < 0.05$ vs the sham group; $^{\wedge}P < 0.05$ vs the sh-NC group; $^{\$}P < 0.05$ vs the miR-140-3p agomir + Oe-NC group.

140-3p to suppress the development of renal fibrosis in a hyperuricemic rat model by promoting CtsD expression. Our research may provide novel targets for the therapeutic strategy of renal fibrosis treatment. However, the molecular mechanisms remain to be explored, and we look forward to further development in the corresponding field.

## Supplementary Data

Supplementary data is available at *Acta Biochimica et Biophysica Sinica* online.

## Funding

This work was supported by the grants from the National Natural Science Foundation of China (No. 82160135), the Hainan Key Research and Development Project (No. ZDYF2022SHFZ016), the Hainan Provincial Natural Science Foundation of China (Nos. 822QN455 and 821MS0825), the Hainan Province Clinical Medical Research Center of NephrologyHainan Province Clinical Medical Center, National Natural Science Fund Cultivating 530 Projects of Hainan General Hospital (Nos. 2021MSXM17, 2021QNXM03, 2021QNXM06, 2021QNXM12, 2021QNXM13 and 2021QNXM17), and the Projects of Hainan General Hospital (Nos. QN202008 and QN202007).

## Conflict of Interest

The authors declare that they have no conflicts of interest.

## References

1. Li M, Jia F, Zhou H, Di J and Yang M. Elevated aerobic glycolysis in renal tubular epithelial cells influences the proliferation and differentiation of podocytes and promotes renal interstitial fibrosis. *Eur Rev Med Pharmacol Sci*, 2018, 22: 5082–5090
2. Lu J, Dalbeth N, Yin H, Li C, Merriman TR, Wei WH. Mouse models for human hyperuricaemia: a critical review. *Nat Rev Rheumatol* 2019, 15: 413–426
3. Yang M, Chen G, Zhang X, Guo Y, Yu Y, Tian L, Chang S, *et al.* Inhibition of class I HDACs attenuates renal interstitial fibrosis in a murine model. *Pharmacol Res* 2019, 142: 192–204
4. Liu M, Liu T, Shang P, Zhang Y, Liu L, Liu T, Sun S. Acetyl-11-keto-β-boswellic acid ameliorates renal interstitial fibrosis via Klotho/TGF-β/Smad signalling pathway. *J Cell Mol Med* 2018, 22: 4997–5007
5. Song Y, Peng C, Lv S, Cheng J, Liu S, Wen Q, Guan G, *et al.* Adipose-derived stem cells ameliorate renal interstitial fibrosis through inhibition of EMT and inflammatory response via TGF-β1 signaling pathway. *Int Immunopharmacol* 2017, 44: 115–122
6. Wang G, Zhang ZJ, Jian WG, Liu PH, Xue W, Wang T, Meng YY, *et al.* Novel long noncoding RNA OTUD6B-AS1 indicates poor prognosis and inhibits clear cell renal cell carcinoma proliferation via the Wnt/β-catenin signaling pathway. *Mol Cancer* 2019, 18: 15
7. Jiang J, Zheng D, Li Y, Liu G, Zhou H and Liu Y. Long noncoding RNA MANTIS relieved the protein-bound uremic toxin-induced injury on human umbilical vein endothelial cells in chronic kidney disease and end-stage renal disease. *Int J Clin Exp Pathol* 2018, 11: 3236–3246
8. Chen W, Zhang L, Zhou ZQ, Ren YQ, Sun LN, Man YL, Ma ZW, *et al.* Effects of long non-coding RNA LINC00963 on renal interstitial fibrosis and oxidative stress of rats with chronic renal failure via the foxo signaling pathway. *Cell Physiol Biochem* 2018, 46: 815–828
9. Wang W, Zhang S, Yang F, Xie J, Chen J, Li Z. Diosmetin alleviates acute kidney injury by promoting the TUG1/Nrf2/HO-1 pathway in sepsis rats. *Int Immunopharmacol* 2020, 88: 106965
10. Long J, Badal SS, Ye Z, Wang Y, Ayanga BA, Galvan DL, Green NH, *et al.* Long noncoding RNA Tug1 regulates mitochondrial bioenergetics in diabetic nephropathy. *J Clin Investigation* 2016, 126: 4205–4218
11. Lei X, Zhang L, Li Z, Ren J. Astragaloside IV/lncRNA-TUG1/TRAF5 signaling pathway participates in podocyte apoptosis of diabetic nephropathy rats. *DDDT* 2018, Volume 12: 2785–2793
12. Zhang B, Zhao C, Hou L, Wu Y. Silencing of the lncRNA *TUG1* attenuates the epithelial-mesenchymal transition of renal tubular epithelial cells by sponging *miR-141-3p* via regulating β-catenin. *Am J Physiol Renal Physiol* 2020, 319: F1125–F1134
13. Riquelme I, Tapia O, Leal P, Sandoval A, Varga MG, Letelier P, Buchegger K, *et al.* miR-101-2, miR-125b-2 and miR-451a act as potential tumor suppressors in gastric cancer through regulation of the PI3K/AKT/mTOR pathway. *Cell Oncol* 2016, 39: 23–33
14. Liao W, Liang P, Liu B, Xu Z, Zhang L, Feng M, Tang Y, *et al.* MicroRNA-140-5p mediates renal fibrosis through TGF-β1/smad signaling pathway by directly targeting TGFBR1. *Front Physiol* 2020, 11: 1093
15. Wu SM, Li TH, Yun H, Ai HW, Zhang KH. miR-140-3p knockdown suppresses cell proliferation and fibrogenesis in hepatic stellate cells via PTEN-mediated AKT/mTOR signaling. *Yonsei Med J* 2019, 60: 561–569
16. Di YQ, Han XL, Kang XL, Wang D, Chen CH, Wang JX, Zhao XF. Autophagy triggers CTSD (cathepsin D) maturation and localization inside cells to promote apoptosis. *Autophagy* 2021, 17: 1170–1192
17. Fox C, Cocchiaro P, Oakley F, Howarth R, Callaghan K, Leslie J, Luli S, *et al.* Inhibition of lysosomal protease cathepsin D reduces renal fibrosis in murine chronic kidney disease. *Sci Rep* 2016, 6: 20101
18. Cocchiaro P, Fox C, Tregidgo NW, Howarth R, Wood KM, Situmorang GR, Pavone LM, *et al.* Lysosomal protease cathepsin D; a new driver of apoptosis during acute kidney injury. *Sci Rep* 2016, 6: 27112
19. Liu N, Wang L, Yang T, Xiong C, Xu L, Shi Y, Bao W, *et al.* EGF receptor inhibition alleviates hyperuricemic nephropathy. *J Am Soc Nephrol* 2015, 26: 2716–2729
20. Zhou H, Qiu ZZ, Yu ZH, Gao L, He JM, Zhang ZW, Zheng J. Paeonol reverses promoting effect of the HOTAIR/miR-124/Notch1 axis on renal interstitial fibrosis in a rat model. *J Cell Physiol* 2019, 234: 14351–14363
21. Zhou Y, Zhang X, Li C, Yuan X, Han L, Li Z, Tan X, *et al.* Research on the pharmacodynamics and mechanism of Fraxini Cortex on hyperuricemia based on the regulation of URAT1 and GLUT9. *Biomed Pharmacother* 2018, 106: 434–442
22. Yokoi H, Mukoyama M, Nagae T, Mori K, Suganami T, Sawai K, Yoshioka T, *et al.* Reduction in connective tissue growth factor by antisense treatment ameliorates renal tubulointerstitial fibrosis. *J Am Soc Nephrol* 2004, 15: 1430–1440
23. Livak KJ, Schmittgen TD. Analysis of relative gene expression data using real-time quantitative PCR and the $2-\Delta\Delta CT$ method. *Methods* 2001, 25: 402–408
24. Zhou Y, Du D, Liu S, Zhao M, Yuan Y, Li L, Chen Y, *et al.* Polyacetylene glycoside attenuates ischemic kidney injury by co-inhibiting inflammation, mitochondria dysfunction and lipotoxicity. *Life Sci* 2018, 204: 55–64
25. Zuo Y, Wang C, Sun X, Hu C, Liu J, Hong X, Shen W, *et al.* Identification of matrix metalloproteinase-10 as a key mediator of podocyte injury and proteinuria. *Kidney Int* 2021, 100: 837–849
26. Gao F, Zhang Y, Yang Z, Wang M, Zhou Z, Zhang W, Ren Y, *et al.* Arctigenin suppressed epithelial-mesenchymal transition through Wnt3a/β-catenin pathway in PQ-induced pulmonary fibrosis. *Front Pharmacol* 2020, 11: 584098
27. Harten SK, Shukla D, Barod R, Hergovich A, Balda MS, Matter K, Esteban MA, *et al.* Regulation of renal epithelial tight junctions by the von Hippel-

Lindau tumor suppressor gene involves occludin and claudin 1 and is independent of E-cadherin. *Mol Biol Cell* 2009, 20: 1089–1101

28. Li H, Xu Y, Zhang Q, Xu H, Xu Y, Ling K. Microvesicles containing miR-34a induce apoptosis of proximal tubular epithelial cells and participate in renal interstitial fibrosis. *Exp Ther Med* 2019, 17: 2310
29. Xu Y, Niu Y, Li H, Pan G. Downregulation of lncRNA TUG1 attenuates inflammation and apoptosis of renal tubular epithelial cell induced by ischemia-reperfusion by sponging miR-449b-5p via targeting HMGB1 and MMP2. *Inflammation* 2020, 43: 1362–1374
30. Han X, Hong Y, Zhang K. TUG1 is involved in liver fibrosis and activation of HSCs by regulating miR-29b. *Biochem Biophys Res Commun* 2018, 503: 1394–1400
31. Sun Q, Luo M, Gao Z, Han X, Yan Z, Xie S, Zhao H, ***et al.*** TUG1 knockdown suppresses cardiac fibrosis after myocardial infarction. *Mamm Genome* 2021, 32: 435–442
32. Ai Y, Chen M, Liu J, Ren L, Yan X, Feng Y. lncRNA TUG1 promotes endometrial fibrosis and inflammation by sponging miR-590-5p to regulate Fasl in intrauterine adhesions. *Int Immunopharmacol* 2020, 86: 106703
33. Yu C, Li L, Xie F, Guo S, Liu F, Dong N, Wang Y. LncRNA TUG1 sponges miR-204-5p to promote osteoblast differentiation through upregulating Runx2 in aortic valve calcification. *Cardiovasc Res* 2018, 114: 168–179
34. Rudnicki M, Perco P, D Haene B, Leierer J, Heinzel A, Mühlberger I, Schweibert N, ***et al.*** Renal microRNA- and RNA-profiles in progressive chronic kidney disease. *Eur J Clin Invest* 2016, 46: 213–226
35. Dong MN, Xiao Y, Li YF, Wang DM, Qu YP, Fang TW, Li H, ***et al.*** Amelioration of paraquat-induced pulmonary fibrosis in mice by regulating miR-140-5p expression with the fibrogenic inhibitor Xuebijing. *Int J Immunopathol Pharmacol* 2020, 34: 205873842092391
36. Singh MP, Sharma C, Kang SC. Morin hydrate attenuates adenine-induced renal fibrosis via targeting cathepsin D signaling. *Int Immunopharmacol* 2021, 90: 107234